Langmuir

Article

pubs.acs.org/Langmuir

Complementary Surface Second Harmonic Generation and Molecular Dynamics Investigation of the Orientation of Organic Dyes at a Liquid/Liquid Interface

Denis Svechkarev,[†,‡] Dmitry Kolodezny,[‡] Sandra Mosquera-Vázquez,[†] and Eric Vauthey*[,†]

[†]Department of Physical Chemistry, University of Geneva, 30 quai Ernest-Ansermet, 1211 Geneva, Switzerland

[‡]Institute for Chemistry, V. N. Karazin Kharkov National University, 4 Svobody Square, 61022 Kharkov, Ukraine

Supporting Information

ABSTRACT: The second-order nonlinear response of two dyes adsorbed at the dodecane/water interface was investigated by surface second harmonic generation (SSHG). These dyes consist of the same chromophoric unit, 2-pyridinyl-5-phenyloxazole, with an alkyl chain located at the two opposite ends. The analysis of the polarization dependence of the SSHG intensity as usually performed points to similar tilt angles of the two dyes with respect to the interface but does not give information on the absolute direction. Molecular dynamics (MD) simulations reveal that both dyes lie almost flat at the interface but have opposite orientations. A refined SSHG data analysis with the width of the orientational distribution yields tilt angles that are in very satisfactory agreement with the MD simulations.

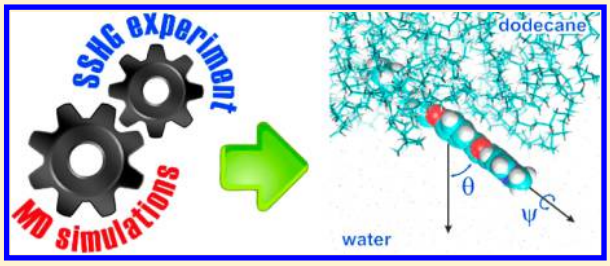

1. INTRODUCTION

Interfaces between two immiscible liquids are ubiquitous in nature and play a crucial role in many technological processes.[1−3] Their specific properties, which often diverge from those of the constituting phases, arise from the asymmetry of the forces acting on this frontier region and from the resulting anisotropic orientations of the interfacial molecules. Therefore, molecules adsorbed at a liquid/liquid interface experience microenvironmental characteristics, such as friction or local electric field, that differ from those of the bulk phases, which are usually described by macroscopic quantities such as viscosity or dielectric constant. This in turn can lead to chemical reactivity that deviates from that observed in bulk solutions. For example, several chemical reactions involving water-insoluble compounds have been shown to proceed faster at the interface with water than in pure organic solvents.[4−6]

Knowledge of the orientation of the molecules adsorbed at the interface is of primary importance for rationalizing their chemical reactivity. However, this information is not readily accessible. In order to probe only the adsorbed solute molecules and not those dissolved in the bulk phases, experimental techniques with high interfacial selectivity have to be used. This is the case of nonlinear optical techniques such as surface second harmonic generation (SSHG)[7−10] and surface sum frequency generation (SSFG),[11,12] which probe the second-order nonlinear optical susceptibility, $\vec{\vec{\chi}}^{(2)}$. Within the dipolar approximation, $\vec{\vec{\chi}}^{(2)}$ vanishes in centrosymmetric media but not at the interface between two isotropic liquids. Moreover, $\vec{\vec{\chi}}^{(2)}$ is frequency-dependent and exhibits resonances at frequencies corresponding to one- or two-photon transitions. SSFG, which is mostly used with one of the optical fields in the infrared to study vibrational resonances, has proven to be particularly powerful for investigating naked interfaces (i.e., interfaces without a solute adsorbed).[13,14] On the other hand, SSHG is usually used in the visible region in resonance with electronic transitions of the adsorbed molecules.[15−19] Electronic SSFG has recently been demonstrated to be a promising alternative for studying adsorbates at air/liquid interfaces.[20,21] Information on the orientation of the adsorbate can be deduced from polarized SSHG experiments.[22−25] However, a number of approximations normally have to be made when analyzing the resulting data to extract orientational information. One of them is the use of a Dirac δ function to describe the angular distribution of the molecules at the interface, which obviously loses its physical meaning when going from a theoretical approach to real systems. This issue has been addressed in several studies,[23,25−28] but the use of an angular distribution is still not systematic. Recently, a novel approach was suggested to obtain the orientational distribution of the transition dipole moments of the adsorbate using a ratio of second harmonic intensities recorded before and after excitation of the molecule with a circularly polarized pump pulse and using particular sets of polarization for the probe and signal fields.[29] However, when pump−probe studies are not feasible, it is not possible to obtain this information from SSHG polarization profiles alone. Additionally, as SSHG is inherently a homodyne technique, the signal intensity is proportional to the square modulus of the susceptibility, $|\vec{\vec{\chi}}^{(2)}|^2$. As a consequence, no information on the

Received: August 5, 2014
Revised: October 30, 2014
Published: October 31, 2014

absolute orientation of the adsorbate (i.e., on which particular end of the molecule is pointing up or down) can be obtained unless heterodyne detection is performed.[21,30]

Alternatively, modern computational methods such as molecular dynamics (MD) can be particularly helpful to gain insight into the interfacial behavior of a solute molecule. Over the past years, MD has been increasingly used to simulate interfaces and interfacial processes,[31−35] for example, adsorption and solvation,[34,36,37] extraction,[38] or the microenvironment of adsorbates.[39,40]

To the best of our knowledge, the determination of the orientation of a solute molecule at a liquid/liquid interface using the combination of polarized SSHG experiments and MD simulations has not been described to date. Here we report on the application of such a combination to study the orientation of two organic dyes consisting of the same pyridine−oxazole−phenyl (POP) chromophoric unit but having an octyl tail attached to the opposite ends at the dodecane/water interface (Figure 1). The chromophore bears donor (alkyloxy) and acceptor (quaternary nitrogen) moieties, thus giving a good perspective for a substantial second-order nonlinear response. The influence of the alkyl chain at both sides of the chromophore on the adsorption at the interface as well as on its orientation are discussed. The results of the MD simulations are compared to the information extracted from the analysis of SSHG polarization profiles and applied to go beyond the assumptions usually used in such SSHG data analysis.

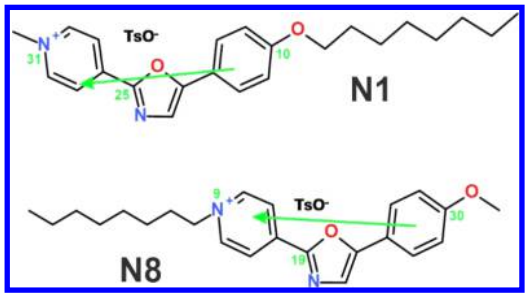

Figure 1. Structures of the dyes, key atom numbers, and calculated $S_1 \leftarrow S_0$ transition dipole moments (green arrows, not to scale).

2. EXPERIMENTAL SECTION

Sample Preparation. The organic dyes, 1-methyl-4-(5-(4-(octyloxy)phenyl)oxazol-2-yl)pyridinium tosylate (**N1**) and 4-(5-(4-methoxyphenyl)oxazol-2-yl)-1-octylpyridinium tosylate (**N8**), were synthesized in the group of Prof. A. O. Doroshenko (V. N. Karazin Kharkov National University) and were used as received. Distilled water and dodecane (pure from Acros Organics) were used without special purification. The absorption spectra were recorded on a Cary 50 spectrophotometer (Varian) in 1 cm quartz cells. The samples for the SSHG experiments were prepared by pouring 10 mL of distilled water into a 4 cm × 4 cm × 4 cm quartz cell along with 100 μL of the dye solution in distilled water (approx. 10^{-4} M) and then adding 12 mL of dodecane. All of the measurements were performed at room temperature.

Surface Second Harmonic Generation. The SSHG measurements were performed using the experimental setup described previously.[41,42] In brief, the probe pulses were generated with a noncollinear optical parametric amplifier (TOPAS-C, Light Conversion) pumped by a 1 kHz Ti:sapphire amplified system (Solstice, Spectra-Physics). About 0.3 μW of the TOPAS output beam was focused through the dodecane phase onto the interface at an angle of incidence of about 70°, where it underwent total internal reflection. The SSHG signal was then collected and focused onto the entrance slit of a Czerny−Turner spectrograph (Shamrock 163, Andor) equipped with a cooled CCD camera (Newton 920, Andor). The illuminated pixels were vertically binned and summed over the wavelength range of interest. In all of the experiments, the polarization of the probe pulse was controlled with a half-wave plate, and the p, s or −45° polarized component of the SSHG signal was detected. The nonresonant contribution to the SSHG signal measured without dye in the aqueous phase was found to be negligibly small.

Quantum-Chemistry Calculations. The ground-state geometries and charge distributions of dodecane, **N1**, and **N8** were optimized using density functional theory (DFT) with the B3LYP functional and the cc-pVDZ basis set as implemented in Gaussian 09.[43] The transition dipole moments of both **N1** and **N8** were calculated using time-dependent DFT (TD-DFT) with the same combination of functional and basis set. The hyperpolarizability tensor elements were computed at the B3LYP/6-31G++(d,p) level at 800 and 1000 nm. These wavelengths were chosen because the experimental and calculated $S_1 \leftarrow S_0$ absorption maxima of both dyes are at 400 and 500 nm, respectively, and thus correspond to two-photon resonances.

Molecular Dynamics Simulations. The MD model of the dodecane/water interface was based on the all-atom CHARMM36 force field for the GROMACS package, version 4.6.5,[44] with the three-site TIP3P water model.[45] The bond lengths and angles for dodecane, **N1**, and **N8** were adapted to the CHARMM force field format with PRODRG.[46] The partial charges necessary to account for Coulomb interactions were derived from the B3LYP/cc-pVDZ electron densities by fitting the electrostatic potential to point (ESP) charges. All of the covalent bonds were constrained to their equilibrium values using the P-LINCS algorithm.[47] The repulsion and dispersion terms of nonbonded interactions were computed using the Lennard-Jones potential energy function. Electrostatics was treated with a particle-mesh Ewald model[48] using a short-range cutoff of 1.0 nm and van der Waals interactions switched off between 0.8 and 1.0 nm. The temperature was maintained using the thermostat by Bussi et al.[49] Periodic boundary conditions were applied, as well as the Berendsen barostat.[50] The simulations were performed with constant number of particles, pressure, and temperature (*NPT* ensemble) using an integration time step of 1 fs with the neighbor list updated every 20 fs. Chloride ions, available in the force field, were used as counterions instead of tosylate ions.

First, a cell containing 267 dodecane molecules was created and equilibrated during 1 ns. In a second stage, two 5 nm × 5 nm × 4 nm cells were added and filled with water (∼6400 molecules) to obtain a 5 nm × 5 nm × 12 nm sandwichlike cell with the dodecane phase in the middle and a water phase on each side along the *z* axis. Because of the periodic boundary conditions adopted here, using only two layers would have led to the formation of two new unwanted dodecane/water interfaces. Additionally, the sandwichlike cell allowed information about the dynamics of **N1** and **N8** to be gathered simultaneously. The volume of the cell also allowed some simulations to be started with the dye molecules located in the bulk phase. A 20 ns trajectory was recorded in every case, allowing enough time for the accumulation of data after adsorption of the dye molecules. Because the motions of the atoms in the MD simulations are random, it was necessary to prepare several starting geometries to analyze all of the most probable cases and to obtain reliable statistical information. Thus, in two cases, the molecules were standing vertically with either their octyl or methyl tail pointing toward the dodecane phase, and three more runs were made with the molecules initially lying flat with respect to the interface. Trajectories were visualized with the VMD package to analyze the behavior of the adsorbed dyes.[51]

Because of the periodic boundary conditions, the molecule could go beyond the cell at one (or more) edges of the cell and virtually appear at its opposite side. In terms of atomic coordinates, this means that the difference between the *x* and *y* coordinates becomes bigger than the cell size, thus artificially increasing the population of molecules lying almost flat with respect to the interface. To address this issue, the analysis algorithm was amended to detect abnormally large *x* and *y* vector coordinates that exceeded a certain threshold, set to be half of the molecule's length. The dimensions of the cell at each step were

dx.doi.org/10.1021/la503121g | *Langmuir* 2014, 30, 13869−13876

then additionally recorded, and the translation procedure was applied when necessary to bring the molecule back to the neighbor virtual cell.

To analyze the molecular orientation at the interface at each time step along the trajectory, vectors going between atoms 10 to 31 and 30 to 9 (Figure 1) were chosen as the z axes for **N1** and **N8**, respectively. These vectors are close to the actual transition dipole moments. Additionally, the xy molecular planes of **N1** and **N8** were defined using atoms 10, 25, and 31 and atoms 30, 19, and 9, respectively. These atoms were chosen to ensure that small torsional rotations of the rings would have very little impact on the directions of the chosen vectors.

3. RESULTS AND DISCUSSION

Spectral Properties. The electronic absorption spectra of the two dyes in water exhibit a broad band with a maximum at approximately 400 nm (Figure 2A), which, as for its well-known analogue 2,5-diphenyloxazole (PPO) and its numerous derivatives, has $\pi-\pi^*$ character and corresponds to the $S_1 \leftarrow S_0$ electronic transition.[52] Figure 2A also shows the stationary SSHG spectra measured with **N1** and **N8** at the dodecane/water interface by tuning the probe wavelength between 800 and 1000 nm. The band maximum is at around 440 nm for both dyes, but the band of **N1** is broader with a shoulder at around 480 nm. Compared with the electronic absorption spectra, both SSHG spectra are red-shifted by about 40 nm (2200 cm^{-1}) and are substantially narrower. Such shifts and bandwidth differences have been observed previously with other dyes such as coumarins.[53−55] Whereas the shift has been ascribed to a solvatochromic effect, the origin of the narrowing has not been totally clarified. In the present case, the absorption spectra of **N1** and **N8** measured in toluene are essentially the same as those in water, and thus, environmental effects cannot be invoked here. However, it should be noted that the enhancement of the SSHG intensity in this spectral region arises from a resonance with a two-photon transition, and therefore, the SSHG spectrum should not only be compared to the linear absorption spectrum but also to the two-photon absorption spectrum, which has been shown to often differ from the one-photon absorption spectrum.[56] The SSHG signal obtained without the dye in the aqueous phase was negligibly small, indicating that the SSHG signal with the dyes has a purely resonant character of dipolar origin.[57] Therefore, the signal intensity depends on the square modulus of the relevant elements of $\vec{\chi}^{(2)}$ and hence on the square of the number of dye molecules contributing to the signal.[19]

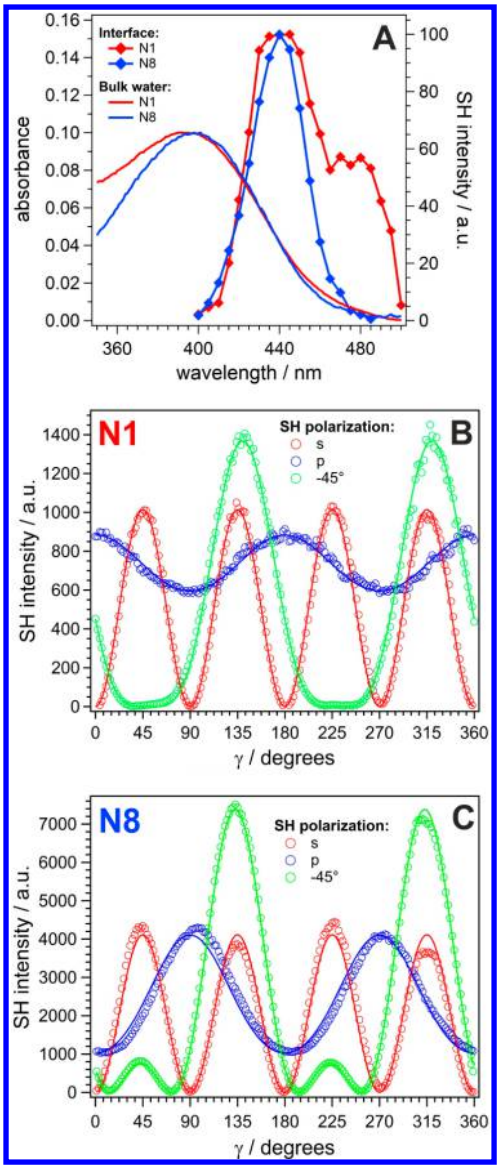

Figure 2. (A) Electronic absorption spectra in water and stationary SSHG spectra (p component) measured at the dodecane/water interface (the polarization of the probe pulse was at 45°). (B, C) Dependences of the intensities of the s, p, and −45° components of the SSHG signals measured at 425 nm for (B) **N1** and (C) **N8** on the polarization angle of the probe field (γ) at the dodecane/water interface. The solid lines show the best fits of the data to eq 1.

Polarized SSHG Experiments. The dependences of the intensities of the s, p, and −45° components of the SSHG signal on the polarization of the probe field at 850 nm measured with both dyes at the dodecane/water interface are shown in Figure 2B and C. The polarization profiles measured at 800 and 1000 nm had the same shape, within the limit of error, excluding the contribution to the measured signal by other species, such as aggregates.[58] If the SSHG spectra in Figure 2A were due to several species, the polarization profiles should vary with the probe wavelength unless all of the species have very similar $\vec{\chi}^{(2)}$ tensors and orientations at the interface, which is very improbable. The solid lines in Figure 2B and C are the best fits to the data of the following equation describing the SSHG intensity:[23,59]

$$I_{SSHG} = C\cdot|a_1\chi^{(2)}_{XXZ}\sin 2\gamma \sin\Gamma + (a_2\chi^{(2)}_{XXZ} + a_3\chi^{(2)}_{ZXX} + a_4\chi^{(2)}_{ZZZ})\cos^2\gamma\cos\Gamma + a_5\chi^{(2)}_{ZXX}\sin^2\gamma\cos\Gamma|^2 I_p{}^2 \quad (1)$$

where C is a constant that depends on the solvents and the probe wavelength; a_i (i = 1−5) are the Fresnel coefficients; $\chi^{(2)}_{XXZ}$, $\chi^{(2)}_{ZXX}$, and $\chi^{(2)}_{ZZZ}$ are the three independent nonzero elements of the second-order susceptibility tensor for a material with a $C_{\infty v}$ symmetry, as is the case for an interface,[8] with the subscripts representing the Cartesian coordinates in the laboratory frame (Figure 3); γ is the polarization angle of the probe field (γ = 0° and 90° for p and s polarization, respectively); Γ is the angle of the polarization component of the SSHG signal (Γ = −45°, 90°, and 0° for the −45°, s, and p components, respectively); and I_p is the intensity of the probe pulse. The Fresnel coefficients were first calculated as described in the Supporting Information, and the relative magnitudes of the three tensor elements were adjusted by using all three polarization profiles simultaneously. The resulting values are listed in Table 1. These values point to substantial differences

dx.doi.org/10.1021/la503121g | Langmuir 2014, 30, 13869−13876

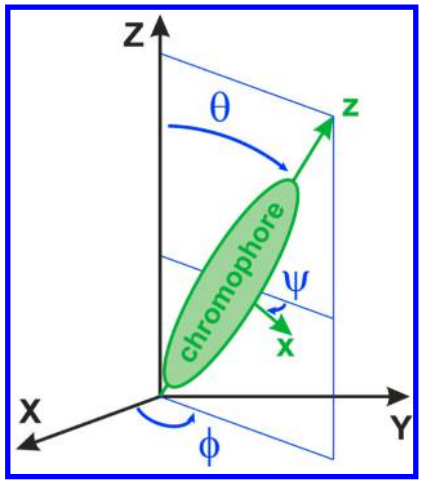

Figure 3. Laboratory and molecular coordinate systems and Euler angles.

between the interfaces with **N1** and **N8** adsorbed, pointing to distinct orientations at the interface. However, as $\vec{\chi}^{(2)}$ is a macroscopic quantity, it does not give direct access to this orientation. For this, one has to consider the microscopic equivalent, which is the second-order polarizability or hyperpolarizability tensor, $\vec{\beta}$:

$$\vec{\chi}^{(2)} \propto N\langle\vec{\beta}\rangle \tag{2}$$

where N is the interfacial adsorbate density and the angle brackets indicate an average over the molecular orientations.

Relating $\vec{\chi}^{(2)}$, represented in the laboratory frame, to $\vec{\beta}$ first requires a molecular coordinate system to be defined. As both **N1** and **N8** belong to the C_1 point group, the long molecular axis of each dye, defined as discussed above, was chosen as the z axis. This axis is also close to parallel to the $S_1 \leftarrow S_0$ transition dipole moment (Figure 1). It has previously been shown that the conformation of a polar tail on a chromophore can noticeably influence the direction and size of the transition dipole moment.[60] A similar effect due to the flexibility of the chromophore could not be ruled out here but was assumed to be negligible. The conjugated π-electronic system thus is located in the xz plane (Figure 3). As the strong $S_1 \leftarrow S_0$ transition in the POP chromophore has $\pi-\pi^*$ character, almost no electronic density redistribution occurs along the y axis upon excitation. As a consequence, the hyperpolarizability tensor elements with a y index should make a negligible contribution.[59] Quantum-chemical calculations of $\vec{\beta}$ at the resonance wavelength were carried out to determine whether the number of relevant tensor elements could be further reduced. The results listed in Table S2 in the Supporting Information indicate that only one tensor element, β_{zzz}, is significant, in good agreement with predictions based on symmetry considerations. In this case, eq 2 can be developed as[59]

$$\chi^{(2)}_{ZXX} = \frac{N}{2\varepsilon_0}\langle\sin^2\theta\cos\theta\rangle\beta_{zzz} \tag{3a}$$

$$\chi^{(2)}_{ZZZ} = \frac{N}{\varepsilon_0}\langle\cos^3\theta\rangle\beta_{zzz} \tag{3b}$$

where the tilt angle θ and the other Euler angles, which describe the orientation of the dye with respect to the interface, are defined in Figure 3.

The orientation parameter D, which directly depends on the tilt angle θ, can be calculated from the following combination of the $\vec{\chi}^{(2)}$ tensor elements:[53,59]

$$D = \frac{\langle\cos^3\theta\rangle}{\langle\cos\theta\rangle} = \frac{\chi^{(2)}_{ZZZ}}{\chi^{(2)}_{ZZZ} + 2\chi^{(2)}_{ZXX}} \tag{4}$$

With the values of the $\vec{\chi}^{(2)}$ tensor elements obtained from the SSHG polarization profiles, D amounts to 0.39 ± 0.03 and 0.21 ± 0.04 for **N1** and **N8**, respectively. The determination of the angle θ from D requires knowledge of $f(\theta)$, the distribution function of θ. In most previous works, a Dirac δ function was used, leading to the simplest case of $D = \cos^2\theta$. Making this assumption here results in θ values of 51.8 ± 1.8° (or 128.2 ± 1.8°) and 63.1 ± 2.6° (or 116.9 ± 2.6°) for **N1** and **N8**, respectively. These two θ values for each dye reflect the two possible directions of the transition dipole moments, i.e., toward the dodecane phase or the aqueous phase. As discussed above, the absolute orientation of the adsorbate cannot be deduced from the polarized SSHG data. For the sake of simplicity, we will henceforth only consider the smallest θ value, which describes the tilt angle of the long molecular axis. The absolute orientation of the molecule will be mentioned when necessary. Such a δ distribution function as assumed here is highly improbable for dyes adsorbed at a liquid/liquid interface, and therefore, the tilt angles obtained with this assumption correspond to lower-limit values.[23] Further information about the orientations of **N1** and **N8** was obtained by performing MD simulations.

MD Simulations. Some of the simulations were performed with the dyes initially located in the aqueous bulk phase. After approximately 1−4 ns, both **N1** and **N8** were adsorbed at the interface and stayed there for the remaining duration of the simulation. The time at which the dye was adsorbed at the interface was chosen as the starting point for the trajectory analysis. In all of the simulations, the dyes had a definite orientation relative to the interface, i.e., with the octyl chain pointing up into the dodecane, down into the aqueous phase, or along the interface. Figure 4A illustrates the variation of the angle θ during 20 ns of simulation. Equilibration can be clearly noticed after about 3 ns. All of the MD results shown in the figures were obtained by starting the simulation with the octyl chain up in the dodecane sulphas. The angle distributions obtained from such trajectories could be well-reproduced using a Gaussian function (Figure 4B,C):[23]

$$f(\theta) = A\exp\left[-\frac{(\theta-\theta_0)^2}{2(\Delta\theta)^2}\right] \tag{5}$$

Table 1. Relative Values of the Nonzero Tensor Elements of $\vec{\chi}^{(2)}$ Obtained from the Fits of Equation 1 to the Polarization Profiles

dye	$\chi^{(2)}_{XXZ}$	$\chi^{(2)}_{ZXX}$	$\chi^{(2)}_{ZZZ}$
N1	(0.90 ± 0.02) + (0.99 ± 0.02)i	(0.65 ± 0.02) + (0.81 ± 0.02)i	(1.00 ± 0.02) + (1.00 ± 0.02)i
N8	(1.57 ± 0.02) + (1.72 ± 0.02)i	(1.36 ± 0.02) + (1.74 ± 0.02)i	(1.00 ± 0.03) + (1.00 ± 0.03)i

dx.doi.org/10.1021/la503121g | *Langmuir* 2014, 30, 13869−13876

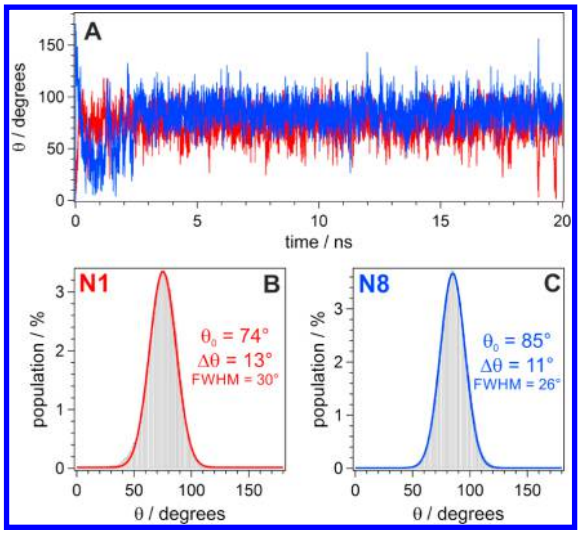

Figure 4. (A) Variation of the tilt angle θ along a whole MD trajectory. (B, C) $f(\theta)$ distributions after equilibration with best fits to eq 5. The full width at half-maximum (FWHM = $2(2 \ln 2)^{1/2}\Delta\theta$) is also given for comparison.

where A is a normalization constant and $\Delta\theta$ and θ_0 are the width (standard deviation) and center of the distribution, respectively. The $\Delta\theta$ and θ_0 values obtained from trajectories with different starting orientations are listed in Table 2. The $f(\theta)$ distributions are essentially independent of the initial orientation and indicate that the orientation with the octyl chain pointing up into the dodecane phase is the most probable, as expected from basic solubility considerations. This implies that the POP chromophores of **N1** and **N8** have opposite orientations at the interface.

Figure 5A,B shows MD snapshots of **N1** and **N8** adsorbed at the interface. The MD simulations, in agreement with the experimental data, indicate that **N8** tends to lie more parallel to the interfacial plane than **N1**. The pyridinium nitrogen, which bears a partial effective positive charge, limits the penetration of the dyes into the dodecane phase. Despite this, a major part of **N1** can be located in this nonpolar environment (Figure 5A). For **N8**, on the other hand, only the octyl chain can penetrate into the dodecane (Figure 5B). However, because of the flexibility of this chain, the chromophic part of **N8** is not fully immersed in the aqueous phase but can adopt an orientation almost parallel to the interface that probably reduces the hydrophobic interactions and also allows the lipophilic methoxy group to interact with the apolar phase (Figure 5C).

The Gaussian distribution $f(\theta)$ obtained from the simulations can now be used instead of the δ function to extract the most probable angle θ_0 from the orientation parameter D (eq 4).[23] The D value of 0.39 ± 0.03 obtained for **N1** results now in θ_0 = 61 ± 2°, whereas the D value of 0.21 ± 0.04 found for **N8** yields θ_0 = 76 ± 4° (see the Supporting Information for details of the procedure). These values obtained by using the physically more realistic angular distributions are now in better agreement with the MD simulations (Table 2). The remaining ~10° difference could be due to various factors: (i) the direction of the $S_1 \leftarrow S_0$ transition dipole moment of the adsorbed dye may differ from that calculated for the equilibrium geometry; (ii) the local temperature in the interfacial region irradiated by the probe beam might be higher than assumed in the MD simulations, leading to a broadening of the angular distribution; (iii) some specific properties of interfacial water may not be well-reproduced by the MD simulations; and (iv) interactions between nearby adsorbates might influence their orientation.

As the hyperpolarizability tensors of both molecules are dominated by a single element, β_{zzz}, no information on the Euler angle ψ, which represents the rotation around the main molecular axis (Figure 3), can be obtained from the SSHG polarization profiles. Figure 6A shows the variation of ψ for both **N1** and **N8** during a 17 ns equilibrated MD trajectory. Although the distribution of ψ is quite broad, there is a clear domination of this angle around 90°, which corresponds to the molecular xz plane facing the interface. One can also notice that the distribution is broader for **N8** than for **N1** and that its center, ψ_0, is not the same in all trajectories (Table 2). This difference in $\Delta\psi$ might arise from the ability of the methoxy end of **N8** to be in either the aqueous phase or the apolar phase, the latter case requiring ψ to depart from 90°. Additionally, the higher friction experienced by **N1** as it penetrates deeper into the dodecane phase, which is substantially more viscous than water ($\eta_{dodecane}$ = 1.37 cP vs η_{water} = 0.89 cP), might decrease the amplitude of the fluctuations of ψ around its most stable value.

Figure 7 gives an even wider look at the dependence of $f(\psi)$ on the tilt angle θ. For molecules with small θ, i.e., with the molecular axis almost perpendicular to the interface, $f(\psi)$ is almost random. However, as θ approaches 90°, the distribution becomes increasingly localized around 90°, i.e., the dye tends to have its molecular plane parallel to the interface. As a consequence, the overall $f(\psi)$ distributions shown in Figure 6B,C are due to the predominance of adsorbates with a large tilt angle.

Table 2. Orientational Parameters Obtained from MD Simulations with Different Initial Orientations of the Dyes and from Polarized SSHG Measurements

		tilt angle				rotation angle			
		N1		N8		N1		N8	
initial orientation	trajectory length (ns)[a]	θ_0	$\Delta\theta$	θ_0	$\Delta\theta$	ψ_0	$\Delta\psi$	ψ_0	$\Delta\psi$
octyl up	17	74	13	85	11	95	28	89	32
octyl down	15.5	75	12	85	11	94	28	91	32
horizontal	16.5	75	12	85	11	95	29	87	32
	19	74	12	85	11	95	28	89	32
	19	76	12	85	11	95	26	90	31
SSHG	–	52	0	63	0				
		61	12	76	11				

[a]After equilibration at the interface.

dx.doi.org/10.1021/la503121g | Langmuir 2014, 30, 13869−13876

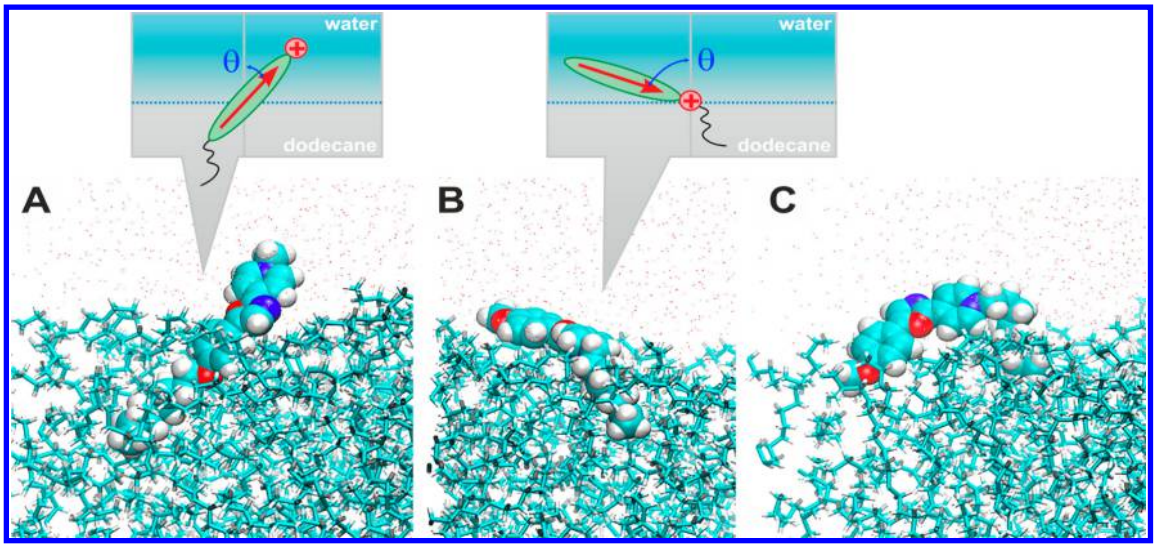

Figure 5. MD snapshots of typical configurations of (A) **N1** and (B, C) **N8** adsorbed at the interface. The phases are turned upside down for better clarity of representation.

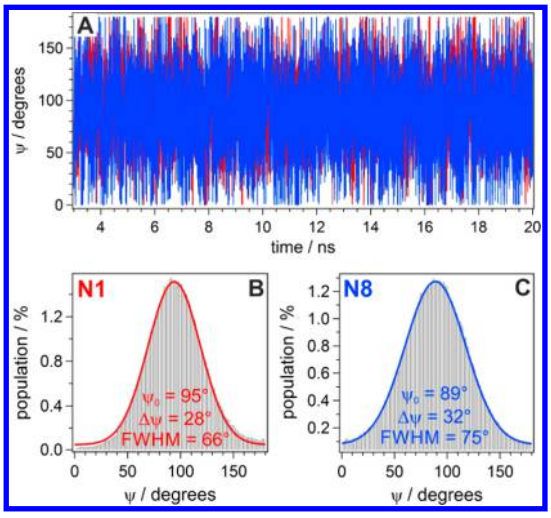

Figure 6. (A) Variation of the angle ψ along the equilibrated part of a trajectory. (B, C) Distributions with the best Gaussian fits.

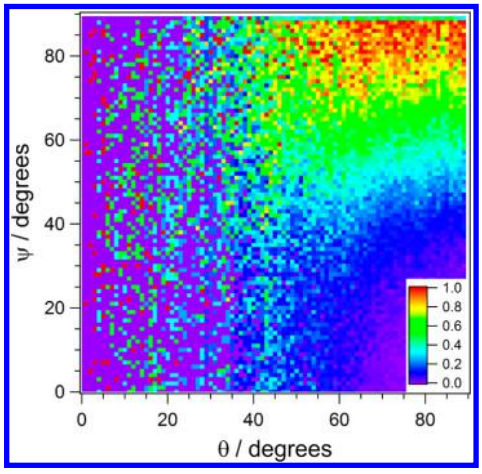

Figure 7. Dependence of the distribution of the angle ψ on the tilt angle θ for **N1** obtained from MD simulations (statistics averaged for all 87 ns of equilibrated trajectories available).

CONCLUDING REMARKS

The above investigation demonstrates that the combination of SSHG spectroscopy and MD simulations is a very powerful method for determining the orientation of organic molecules adsorbed at liquid/liquid interfaces. We investigated two molecules consisting of the same chromophoric unit but with an aliphatic chain located at the two opposite ends. From the analysis of the polarized SSHG measurements alone, only relatively minor differences in the tilt angle between the long molecular axis of the dyes and the interface normal were obtained, pointing a priori to similar orientations. On the other hand, MD simulations showed that the two dyes are oriented in opposite directions, as expected from the positions of the alkyl chain, and they allowed the distribution of the tilt angle to be determined. Using the width of this distribution to refine the analysis of the polarized SSHG measurements yielded tilt angles that are in very satisfactory agreement with those obtained from the MD simulations, although smaller in both cases by about 10°. This difference is most likely due to the various assumptions made in the SSHG data analysis and to several effects not taken into account in the MD simulations.

ASSOCIATED CONTENT

Supporting Information

Calculation of the Fresnel coefficients and details of the analysis of polarized SSHG data; dependence of the distribution of ψ on the tilt angle θ for **N8**; and topologies of dodecane and both dyes used for MD simulations. This material is available free of charge via the Internet at http://pubs.acs.org.

AUTHOR INFORMATION

Corresponding Author

*E-mail: Eric.Vauthey@unige.ch.

Notes

The authors declare no competing financial interest.

ACKNOWLEDGMENTS

We are thankful to Prof. P.-F. Brevet (Institut Lumière Matière, Université Lyon 1) for fruitful discussions and to O. Borodin and R. Iliashenko (V. N. Karazin Kharkov National University)

for providing the compounds for study. This work was supported by the Swiss National Science Foundation through Project 200020-147098 and the University of Geneva. D.S. and D.K. also thank the Swiss Federal Commission for Scholarships and the Ministry of Education and Science of Ukraine, respectively, for supporting their stays in Switzerland.

REFERENCES

(1) Volkov, A. G. E. *Liquid Interfaces in Chemical, Biological, and Pharmaceutical Applications*; Marcel Dekker: New York, 2009.
(2) Watarai, H.; Teramae, N.; Sawada, T. *Interfacial Nanochemistry*; Kluwer Academic: New York, 2005.
(3) Adamson, A. W.; Gast, A. P. *Physical Chemistry of Surfaces*, 6th ed.; Wiley: New York, 1997.
(4) Breslow, R. Hydrophobic Effects on Simple Organic Reactions in Water. *Acc. Chem. Res.* **1991**, *24*, 159−164.
(5) Narayan, S.; Muldoon, J.; Finn, M. G.; Fokin, V. V.; Kolb, H. C.; Sharpless, K. B. "On Water": Unique Reactivity of Organic Compounds in Aqueous Suspension. *Angew. Chem., Int. Ed.* **2005**, *44*, 3275−3279.
(6) Jung, Y.; Marcus, R. A. On the Theory of Organic Catalysis "on Water". *J. Am. Chem. Soc.* **2007**, *129*, 5492−5502.
(7) Corn, R. M.; Higgins, D. A. Optical Second Harmonic Generation as a Probe of Surface Chemistry. *Chem. Rev.* **1994**, *94*, 107−125.
(8) Eisenthal, K. B. Liquid Interfaces Probed by Second-Harmonic and Sum-Frequency Spectroscopy. *Chem. Rev.* **1996**, *96*, 1343−1360.
(9) Richert, S.; Fedoseeva, M.; Vauthey, E. Ultrafast Photoinduced Dynamics at Air/Liquid and Liquid/Liquid Interfaces. *J. Phys. Chem. Lett.* **2012**, *3*, 1635−1642.
(10) Nihonyanagi, S.; Mondal, J. A.; Yamaguchi, S.; Tahara, T. Structure and Dynamics of Interfacial Water Studied by Heterodyne-Detected Vibrational Sum-Frequency Generation. *Annu. Rev. Phys. Chem.* **2014**, *64*, 579−603.
(11) Richmond, G. L. Molecular Bonding and Interactions at Aqueous Surfaces as Probed by Vibrational Sum Frequency Spectroscopy. *Chem. Rev.* **2002**, *102*, 2693−2724.
(12) Shultz, M. J.; Schnitzer, C.; Simonelli, D.; Baldelli, S. Sum Frequency Generation Spectroscopy of the Aqueous Interface. Ionic and Soluble Molecular Solutions. *Int. Rev. Phys. Chem.* **2000**, *19*, 123−153.
(13) McGuire, J.; Shen, Y. R. Ultrafast Vibrational Dynamics at Water Interfaces. *Science* **2006**, *313*, 1945−1948.
(14) Zhang, Z.; Piatkowski, L.; Bakker, H. J.; Bonn, M. Ultrafast Vibrational Energy Transfer at the Water/Air Interface Revealed by Two-Dimensional Surface Vibrational Spectroscopy. *Nat. Chem.* **2011**, *3*, 888−893.
(15) Steel, W. H.; Walker, R. A. Measuring Dipolar Width across Liquid−Liquid Interfaces with "Molecular Rulers". *Nature* **2003**, *424*, 296−299.
(16) Fujiwara, K.; Wada, S.; Monjushiro, H.; Watarai, H. Ion-Association Aggregation of an Anionic Porphyrin at the Liquid/Liquid Interface Studied by Second Harmonic Generation Spectroscopy. *Langmuir* **2006**, *22*, 2482−2486.
(17) McArthur, E. A.; Eisenthal, K. B. Ultrafast Excited-State Electron Transfer at an Organic Liquid/Aqueous Interface. *J. Am. Chem. Soc.* **2006**, *128*, 1068−1069.
(18) Onorato, R. M.; Otten, D. E.; Saykally, R. J. Adsorption of Thiocyanate Ions to the Dodecanol/Water Interface Characterized by UV Second Harmonic Generation. *Proc. Natl. Acad. Sci. U.S.A.* **2009**, *106*, 15176−15180.
(19) Fedoseeva, M.; Richert, S.; Vauthey, E. Excited-State Dynamics of Organic Dyes at Liquid−Liquid Interfaces. *Langmuir* **2012**, *28*, 11291−11301.
(20) Yamaguchi, S.; Tahara, T. Precise Electronic $\chi^{(2)}$ Spectra of Molecules Adsorbed at an Interface Measured by Multiplex Sum Frequency Generation. *J. Phys. Chem. B* **2004**, *108*, 19079−19082.
(21) Yamaguchi, S.; Tahara, T. Heterodyne-Detected Electronic Sum Frequency Generation: "Up" versus "Down" Alignment of Interfacial Molecules. *J. Chem. Phys.* **2008**, *129*, No. 101102.
(22) Grubb, S. G.; Kim, M. W.; Rasing, T.; Shen, Y. R. Orientation of Molecular Monolayers at the Liquid−Liquid Interface As Studied by Optical Second Harmonic Generation. *Langmuir* **1988**, *4*, 452−454.
(23) Tamburello-Luca, A. A.; Hebert, P.; Brevet, P. F.; Girault, H. H. Resonant-Surface Second-Harmonic Generation Studies of Phenol Derivatives at Air/Water and Hexane/Water Interfaces. *J. Chem. Soc., Faraday Trans.* **1996**, *92*, 3079−3085.
(24) Salafsky, J. S.; Eisenthal, K. B. Second Harmonic Spectroscopy: Detection and Orientation of Molecules at a Biomembrane Interface. *Chem. Phys. Lett.* **2000**, *319*, 435−439.
(25) Gonella, G.; Dai, H.-L.; Fry, H. C.; Therien, M. J.; Krishnan, V.; Tronin, A.; Blasie, J. K. Control of the Orientational Order and Nonlinear Optical Response of the "Push−Pull" Chromophore RuPZn via Specific Incorporation into Densely Packed Monolayer Ensembles of an Amphiphilic 4-Helix Bundle Peptide: Second Harmonic Generation at High Chromophore Densities. *J. Am. Chem. Soc.* **2010**, *132*, 9693−9700.
(26) Mitchell, S. A. Indole Adsorption to a Lipid Monolayer Studied by Optical Second Harmonic Generation. *J. Phys. Chem. B* **2009**, *113*, 10693−10707.
(27) Simpson, G. J.; Rowlen, K. L. An SHG Magic Angle: Dependence of Second Harmonic Generation Orientation Measurements on the Width of the Orientation Distribution. *J. Am. Chem. Soc.* **1999**, *121*, 2635−2636.
(28) Sen, S.; Yamaguchi, S.; Tahara, T. Different Molecules Experience Different Polarities at the Air/Water Interface. *Angew. Chem., Int. Ed.* **2009**, *48*, 6439−6442.
(29) Rao, Y.; Hong, S.-Y.; Turro, N. J.; Eisenthal, K. B. Molecular Orientational Distribution at Interfaces Using Second Harmonic Generation. *J. Phys. Chem. C* **2011**, *115*, 11678−11683.
(30) Kemnitz, K.; Bhattacharyya, K.; Hicks, J. M.; Pinto, G. R.; Eisenthal, K. B.; Heinz, T. F. The Phase of Second-Harmonic Light Generated at an Interface and Its Relation to Absolute Molecular Orientation. *Chem. Phys. Lett.* **1986**, *131*, 285−290.
(31) Benjamin, I. Molecular Structure and Dynamics at Liquid−Liquid Interfaces. *Annu. Rev. Phys. Chem.* **1997**, *48*, 407−451.
(32) Rivera, J.; McCabe, C.; Cummings, P. Molecular Simulations of Liquid−Liquid Interfacial Properties: Water−*n*-Alkane and Water−Methanol−*n*-Alkane Systems. *Phys. Rev. E* **2003**, *67*, No. 011603.
(33) Wang, Y.; Hodas, N. O.; Jung, Y.; Marcus, R. A. Microscopic Structure and Dynamics of Air/Water Interface by Computer Simulations—Comparison with Sum-Frequency Generation Experiments. *Phys. Chem. Chem. Phys.* **2011**, *13*, 5388−5393.
(34) Wernersson, E.; Heyda, J.; Vazdar, M.; Lund, M.; Mason, P. E.; Jungwirth, P. Orientational Dependence of the Affinity of Guanidinium Ions to the Water Surface. *J. Phys. Chem. B* **2011**, *115*, 12521−12526.
(35) Razavi, S.; Koplik, J.; Kretzschmar, I. Molecular Dynamics Simulations: Insight into Molecular Phenomena at Interfaces. *Langmuir* **2014**, *30*, 11272−11283.
(36) Pohorille, A.; Benjamin, I. Molecular Dynamics of Phenol at the Liquid−Vapor Interface of Water. *J. Chem. Phys.* **1991**, *94*, 5599−5605.
(37) Kundu, A.; Watanabe, H.; Yamaguchi, S.; Tahara, T. Agreement between Experimentally and Theoretically Estimated Orientational Distributions of Solutes at the Air/Water Interface. *J. Phys. Chem. C* **2013**, *117*, 8887−8891.
(38) Zheng, H.-d.; Wu, F.-d.; Wang, B.-y.; Wu, Y.-x. Molecular Dynamics Simulation on the Interfacial Features of Phenol Extraction by TBP/Dodecane in Water. *Comput. Theor. Chem.* **2011**, *970*, 66−72.
(39) Beierlein, F.; Krause, A.; Jaeger, C. M.; Fita, P.; Vauthey, E.; Clark, T. Molecular-Dynamics Simulations of Liquid Phase Interfaces: Understanding the Structure of the Glycerol/Water−Dodecane System. *Langmuir* **2013**, *29*, 11898−11907.
(40) Richert, S.; Mosquera Vazquez, S.; Grzybowski, M.; Gryko, D. T.; Kyrychenko, A.; Vauthey, E. Excited-State Dynamics of an Environment-Sensitive Push−Pull Diketopyrrolopyrrole: Major Differ-

ences between the Bulk Solution Phase and the Dodecane/Water Interface. *J. Phys. Chem. B* **2014**, *118*, 9952−9963.
(41) Fedoseeva, M.; Letrun, R.; Vauthey, E. Excited-State Dynamics of Rhodamine 6G in Aqueous Solution and at the Dodecane/Water Interface. *J. Phys. Chem. B* **2014**, *118*, 5184−5193.
(42) Fedoseeva, M.; Fita, P.; Vauthey, E. Excited-State Dynamics of Charged Dyes at Alkane/Water Interfaces in the Presence of Salts and Ionic Surfactants. *Langmuir* **2013**, *29*, 14865−14872.
(43) Frisch, M. J.; Trucks, G. W.; Schlegel, H. B.; Scuseria, G. E.; Robb, M. A.; Cheeseman, J. R.; Scalmani, G.; Barone, V.; Mennucci, B.; Petersson, G. A., et al. *Gaussian 09*, revision C1; Gaussian, Inc.: Wallingford, CT, 2009.
(44) Pronk, S.; Páll, S.; Schulz, R.; Larsson, P.; Bjelkmar, P.; Apostolov, R.; Shirts, M. R.; Smith, J. C.; Kasson, P. M.; van der Spoel, D.; et al. GROMACS 4.5: A High-Throughput and Highly Parallel Open Source Molecular Simulation Toolkit. *Bioinformatics* **2013**, *29*, 845−854.
(45) Jorgensen, W. L.; Chandrasekhar, J.; Madura, J. D.; Impey, R. W.; Klein, M. L. Comparison of Simple Potential Functions for Simulating Liquid Water. *J. Chem. Phys.* **1983**, *79*, 926−935.
(46) Schüttelkopf, A. W.; van Aalten, D. M. F. PRODRG: A Tool for High-Throughput Crystallography of Protein−Ligand Complexes. *Acta Crystallogr., Sect. D* **2004**, *60*, 1355−1363.
(47) Hess, B. P-Lincs: A Parallel Linear Constraint Solver for Molecular Simulation. *J. Chem. Theory Comput.* **2008**, *4*, 116−122.
(48) Essmann, U.; Perera, L.; Berkowitz, M. L.; Darden, T.; Lee, H.; Pedersen, L. G. A Smooth Particle Mesh Ewald Method. *J. Chem. Phys.* **1995**, *103*, 8577−8593.
(49) Bussi, G.; Zykova-Timan, T.; Parrinello, M. Isothermal−Isobaric Molecular Dynamics Using Stochastic Velocity Rescaling. *J. Chem. Phys.* **2009**, *130*, No. 074101.
(50) Berendsen, H. J. C.; Postma, J. P. M.; van Gunsteren, W. F.; DiNola, A.; Haak, J. R. Molecular Dynamics with Coupling to an External Bath. *J. Chem. Phys.* **1984**, *81*, 3684−3690.
(51) Humphrey, W.; Dalke, A.; Schulten, K. VMD: Visual Molecular Dynamics. *J. Mol. Graphics* **1996**, *14*, 33−38.
(52) Ponomarev, O. A.; Brusil'tsev, Y. N.; Kotelevskii, S. I.; Mitina, V. G.; Pedash, Y. F. Nature of the Excited States of Dialkylamino Derivatives of Aromatic and Heteroaromatic Compounds with an Annelated Oxazole Ring. *Theor. Exp. Chem.* **1991**, *26*, 605−611.
(53) Pant, D.; Le Guennec, M.; Illien, B.; Girault, H. H. The pH Dependent Adsorption of Coumarin 343 at the Water/Dichloroethane Interface. *Phys. Chem. Chem. Phys.* **2004**, *6*, 3140−3146.
(54) Benderskii, A. V.; Eisenthal, K. B. Aqueous Solvation Dynamics at the Anionic Surfactant Air/Water Interface. *J. Phys. Chem. B* **2001**, *105*, 6698−6703.
(55) Zimdars, D.; Eisenthal, K. B. Static and Dynamic Solvation at the Air/Water Interface. *J. Phys. Chem. B* **2001**, *105*, 3993−4002.
(56) Makarov, N. S.; Drobizhev, M.; Rebane, A. Two-Photon Absorption Standards in the 550−1600 nm Excitation Wavelength Range. *Opt. Express* **2008**, *16*, 4029−4047.
(57) Shen, Y. R. Surface Contribution versus Bulk Contribution in Surface Nonlinear Optical Spectroscopy. *Appl. Phys. B: Lasers Opt.* **1999**, *68*, 295−300.
(58) Fita, P.; Fedoseeva, M.; Vauthey, E. Hydrogen-Bond-Assisted Excited-State Deactivation at Liquid/Water Interfaces. *Langmuir* **2011**, *27*, 4645−4652.
(59) Brevet, P.-F. *Surface Second Harmonic Generation*; Presses Polytechniques et Universitaires Romandes: Lausanne, Switzerland, 1997.
(60) Brand, C.; Meerts, W. L.; Schmitt, M. How and Why Do Transition Dipole Moment Orientations Depend on Conformer Structure? *J. Phys. Chem. A* **2011**, *115*, 9612−9619.